Analysis of a low-energy correction to the eikonal approximation

Tokuro Fukui,[1,*] Kazuyuki Ogata,[1,†] and Pierre Capel[2,‡]

[1]*Research Center for Nuclear Physics, Osaka University, Ibaraki, Osaka 567-0047, Japan*

[2]*Physique Nucléaire et Physique Quantique C.P. 229, Université Libre de Bruxelles (ULB), B-1050, Brussels, Belgium*

(Received 27 January 2014; revised manuscript received 29 July 2014; published 22 September 2014)

Extensions of the eikonal approximation to low energy (20 MeV/nucleon typically) are studied. The relation between the dynamical eikonal approximation (DEA) and the continuum-discretized coupled-channels method with the eikonal approximation (E-CDCC) is discussed. When Coulomb interaction is artificially turned off, DEA and E-CDCC are shown to give the same breakup cross section, within 3% error, of ^{15}C on ^{208}Pb at 20 MeV/nucleon. When the Coulomb interaction is included, the difference is appreciable and none of these models agrees with full CDCC calculations. An empirical correction significantly reduces this difference. In addition, E-CDCC has a convergence problem. By including a quantum-mechanical correction to E-CDCC for lower partial waves between ^{15}C and ^{208}Pb, this problem is resolved and the result perfectly reproduces full CDCC calculations at a lower computational cost.

DOI: 10.1103/PhysRevC.90.034617 PACS number(s): 24.10.−i, 25.60.Gc, 21.10.Gv, 27.20.+n

I. INTRODUCTION

The development of radioactive-ion beams in the mid-1980s has enabled the exploration of the nuclear landscape far from stability. This technical breakthrough has led to the discovery of exotic nuclear structures, like nuclear halos and shell inversions. Halo nuclei exhibit a very large matter radius compared to their isobars. This unusual feature is explained by a strongly clusterized structure: a compact core that contains most of the nucleons to which one or two neutrons are loosely bound. Due to quantum tunneling, these valence neutrons exhibit a large probability of presence at a large distance from the core, hence increasing significantly the radius of the nucleus. Examples of one-neutron halo nuclei are ^{11}Be and ^{15}C, while ^{6}He and ^{11}Li exhibit two neutrons in their halo. Though less probable, proton halos are also possible. The exotic halo structure has thus been the subject of many theoretical and experimental studies for the last 30 years [1,2].

Due to their very short lifetime, halo nuclei must be studied through indirect techniques, such as reactions. The most widely used reaction to study halo nuclei is the breakup reaction, in which the halo dissociates from the core through the interaction with a target. The extraction of reliable structure information from measurements requires a good understanding of the reaction process. Various models have been developed to describe the breakup of two-body projectiles, i.e., one-nucleon halo nuclei (see Ref. [3] for a review).

The continuum-discretized coupled channel method (CDCC) is a fully quantum model in which the wave function describing the three-body motion—two-body projectile plus target—is expanded over the projectile eigenstates [4–6]. For breakup modeling, the core-halo continuum must be included and hence is discretized and truncated to form an approximate complete set of states. With such an expansion, the corresponding Schrödinger equation translates into a set of coupled equations [6–8]. This reaction model is very general and has been successfully used to describe several real and virtual breakup reactions at both low and intermediate energies [9–12]. However, it can be very computationally challenging, especially at high beam energy. This hinders the extension of CDCC models to reactions beyond the simple usual two-body description of the projectile. Simplifying approximations, less computationally demanding, can provide an efficient way to avoid that limitation of CDCC.

At sufficiently high energy, the eikonal approximation can be performed. In that approximation, the projectile-target relative motion is assumed not to deviate significantly from the asymptotic plane wave [13]. By factorizing that plane wave out of the three-body wave function, the Schrödinger equation can be significantly simplified. Both the eikonal CDCC (E-CDCC) [14,15] and the dynamical eikonal approximation (DEA) [16,17] are such eikonal models. Note that these models differ from the usual eikonal approximation in that they do not include the subsequent adiabatic approximation, in which the internal dynamics of the projectile is neglected [18].

The E-CDCC model solves the eikonal equation using the same discretization technique as the full CDCC model. Thanks to this, E-CDCC can be easily extended to a hybrid version, in which a quantum-mechanical (QM) correction to the scattering amplitude can be included for the low orbital angular momentum L between the projectile and the target. This helps in obtaining results as accurate as a full CDCC with a minimal task. In addition, E-CDCC can take the dynamical relativistic effects into account [19,20], and it has recently been extended to inclusive breakup processes [21,22].

Within the DEA, the eikonal equation is solved by expanding the projectile wave function upon a three-dimensional mesh, i.e., without the CDCC partial-wave expansion [16]. This prescription is expected to efficiently include components of the projectile wave function up to high orbital angular momentum between its constituents. Moreover, it enables describing both bound and breakup states on the same footing, without resorting to continuum discretization. Since DEA

*tokuro@rcnp.osaka-u.ac.jp

†kazuyuki@rcnp.osaka-u.ac.jp

‡pierre.capel@ulb.ac.be

treats the three-body dynamics explicitly, all coupled-channels effects are automatically included. Excellent agreement with the experiment has been obtained at the DEA for the breakup and elastic scattering of one-nucleon halo nuclei on both heavy and light targets at intermediate energies (e.g., 70 MeV/nucleon) [17].

In a recent work [23], a comparison between CDCC and DEA was performed. The breakup of the one-neutron halo nucleus ^{15}C on ^{208}Pb has been chosen as a test case. At 68 MeV/nucleon, the results of the two models agree very well with each other. At 20 MeV/nucleon, DEA cannot reproduce the CDCC results because the eikonal approximation is no longer valid at such low energy. It appears that the problem is due to the Coulomb deflection, which, at low energy significantly distorts the projectile-target relative motion from a pure plane wave. Because of the computational advantage of the eikonal approximation over the CDCC framework, it is important to pin down where the difference comes from in more detail and try to find a way to correct it.

The goal of the present paper is to analyze in detail the QM correction to E-CDCC in its hybrid version to see if it can be incorporated within the DEA to correct the lack of Coulomb deflection observed in that reaction model. To do so, we compare E-CDCC and DEA with a special emphasis upon their treatment of the Coulomb interaction. We focus on the ^{15}C breakup on ^{208}Pb at 20 MeV/nucleon. First, we compare the results of DEA and E-CDCC with the Coulomb interaction turned off to show that both models solve essentially the same Schrödinger equation. Then we include the Coulomb interaction to confirm the Coulomb deflection effect observed by the authors of Ref. [23]. We check that the hybrid version of E-CDCC reproduces correctly the full CDCC calculations, and analyze this QM correction to suggest an approximation that can be implemented within DEA to simulate the Coulomb deflection.

In Sec. II we briefly review DEA and E-CDCC, and clarify the relation between them. We compare in Sec. III the breakup cross sections of ^{15}C on ^{208}Pb at 20 MeV/nucleon, with and without the Coulomb interaction. A summary is given in Sec. IV.

II. FORMALISM

A. Three-body reaction system

We describe the ^{15}C breakup on ^{208}Pb using the coordinate system shown in Fig. 1. The coordinate of the center of mass (c.m.) of ^{15}C relative to ^{208}Pb is denoted by $\boldsymbol{R}$, and $\boldsymbol{r}$ is the neutron-^{14}C relative coordinate. $\boldsymbol{R}_n$ and $\boldsymbol{R}_{14}$ are, respectively, the coordinates of the neutron n and the c.m. of ^{14}C from ^{208}Pb. We assume both ^{14}C and ^{208}Pb to be inert nuclei. In this study we neglect the spin of n. The Hamiltonian describing the ^{15}C structure therefore reads

$$h = -\frac{\hbar^2}{2\mu_{n14}}\Delta_{\boldsymbol{r}} + U_{nC}(\boldsymbol{r}), \tag{1}$$

where μ_{n14} is the ^{14}C-n reduced mass and U_{nC} is a phenomenological potential describing the ^{14}C-n interaction (see Sec. III A). We denote by $\varphi_{\varepsilon\ell m}$ the eigenstates of Hamiltonian of Eq. (1) at energy ε in partial wave ℓm, with ℓ the ^{14}C-n orbital angular momentum and m its projection. For negative energies, these states are discrete and describe bound states of the nucleus. For the present comparison, we consider the sole ground state $\varphi_{0\ell_0 m_0}$ at energy $\varepsilon_0 = -1.218$ MeV. The positive-energy eigenstates correspond to continuum states that simulate the broken up projectile.

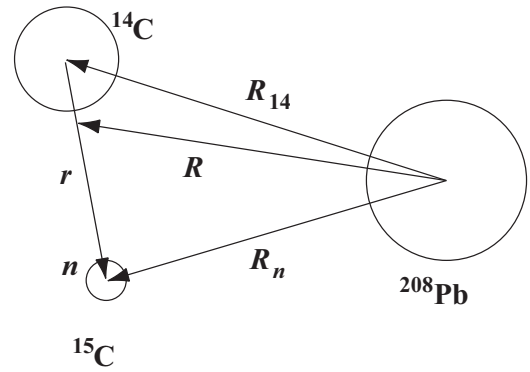

FIG. 1. Schematic illustration of the $(^{14}\mathrm{C}+n)+{}^{208}$Pb three-body system.

To simulate the interaction between n (^{14}C) and ^{208}Pb, we adopt the optical potential U_n (U_{14}) (see Sec. III A). Within this framework, the study of ^{15}C-^{208}Pb collision reduces to solving the three-body Schrödinger equation

$$H\Psi(\boldsymbol{R},\boldsymbol{r}) = E_{\mathrm{tot}}\Psi(\boldsymbol{R},\boldsymbol{r}) \tag{2}$$

with the Hamiltonian

$$H = -\frac{\hbar^2}{2\mu}\Delta_{\boldsymbol{R}} + h + U_{14}(\boldsymbol{R}_{14}) + U_n(\boldsymbol{R}_n), \tag{3}$$

where μ is the ^{15}C-^{208}Pb reduced mass. Equation (2) has to be solved with the incoming boundary condition

$$\lim_{z\to-\infty}\Psi(\boldsymbol{R},\boldsymbol{r}) = e^{iK_0 z+\cdots}\varphi_{0\ell_0 m_0}(\boldsymbol{r}), \tag{4}$$

where K_0 is the wave number for the initial projectile-target motion, whose direction defines the z axis. That wave number is related to the total energy $E_{\mathrm{tot}} = \hbar^2 K_0^2/(2\mu) + \varepsilon_0$. The "$\cdots$" in Eq. (4) indicates that the projectile-target relative motion is distorted by the Coulomb interaction, even at large distances.

In the eikonal approximation, the three-body wave function Ψ is assumed not to vary significantly from the incoming plane wave of Eq. (4). Hence the usual eikonal factorization

$$\Psi(\boldsymbol{R},\boldsymbol{r}) = e^{iK_0 z}\psi(\boldsymbol{b},z,\boldsymbol{r}), \tag{5}$$

where we have explicitly decomposed $\boldsymbol{R}$ in its longitudinal z and transverse $\boldsymbol{b}$ components. In the following $\boldsymbol{b}$ is expressed as $\boldsymbol{b} = (b,\phi_R)$ with b the impact parameter and ϕ_R the azimuthal angle of $\boldsymbol{R}$.

Using factorization Eq. (5) in Eq. (2) and taking into account that ψ varies smoothly with $\boldsymbol{R}$, we obtain equations simpler to solve than the full three-body Schrödinger equation (2). In the following subsections, we specify the equations solved within the E-CDCC (Sec. II B) and the DEA (Sec. II C).

B. Continuum-discretized coupled-channels method with the eikonal approximation

E-CDCC expresses the three-body wave function Ψ as [14,15]

$$\Psi(\boldsymbol{R},\boldsymbol{r}) = \sum_{i\ell m} \bar{\xi}_{i\ell m}(b,z)\varphi_{i\ell m}(\boldsymbol{r})e^{iK_i z}e^{i(m_0-m)\phi_R}\phi_i^{\mathrm{C}}(R), \quad (6)$$

where $\{\varphi_{i\ell m}\}$ are square-integrable states that describe the eigenstates of Hamiltonian h Eq. (1). The subscript i labels the eigenenergy of ^{15}C. The ground state corresponds to $i = 0$ and the corresponding wave function $\varphi_{0\ell_0 m_0}$ is the exact eigentstate of h. The values $i > 0$ correspond to discrete states simulating ^{15}C continuum. They are obtained by the binning technique [24], viz by averaging exact continuum states over small positive-energy intervals, or bins. The set $\{\varphi_{i\ell m}\}$ satisfying

$$\langle\varphi_{i'\ell'm'}\,|h|\,\varphi_{i\ell m}\rangle_{\boldsymbol{r}} = \varepsilon_i\delta_{i'i}\delta_{\ell'\ell}\delta_{m'm} \quad (7)$$

is assumed to form an approximate complete set for the projectile internal coordinate $\boldsymbol{r}$. The plane wave $e^{iK_i z}$ contains the dominant part of the projectile-target motion as explained above. The corresponding wave number varies with the energy of the eigenstate of ^{15}C respecting the conservation of energy $E_{\mathrm{tot}} = \hbar^2K_i^2/2\mu + \varepsilon_i$. In Eq. (6), ϕ_i^{C} is the approximate Coulomb incident wave function given by

$$\phi_i^{\mathrm{C}}(R) = e^{i\eta_i \ln[K_i R - K_i z]}, \quad (8)$$

where η_i is the Sommerfeld parameter corresponding to the ith state of ^{15}C

$$\eta_i = \frac{Z_{\mathrm{C}}Z_{\mathrm{T}}e^2\mu}{\hbar^2K_i}, \quad (9)$$

with $Z_{\mathrm{C}}e$ ($Z_{\mathrm{T}}e$) the charge of the projectile (target). The functions $\bar{\xi}$ are the coefficients of the expansion Eq. (6) that have to be evaluated numerically.

Inserting Eq. (6) into Eq. (2), multiplied by $\varphi_{i'\ell'm'}$ on the left, and integrating over $\boldsymbol{r}$, one gets [14,15]

$$\frac{\partial}{\partial z}\bar{\xi}_c(b,z) = \frac{1}{i\hbar v_i(R)}\sum_{c'}\mathcal{F}_{cc'}(b,z)\bar{\xi}_{c'}(b,z)e^{i(K_{i'}-K_i)z}\mathcal{R}_{ii'}(b,z), \quad (10)$$

where the index c denotes i, ℓ, and m together. In E-CDCC, the projectile-target velocity v_i depends on both the projectile excitation energy and its position following

$$v_i(R) = \frac{1}{\mu}\sqrt{\hbar^2K_i^2 - 2\mu V_{\mathrm{C}}(R)}, \quad (11)$$

where

$$V_{\mathrm{C}}(R) = \frac{Z_{\mathrm{C}}Z_{\mathrm{T}}e^2}{R} \quad (12)$$

is the projectile-target potential that slows down the projectile as it approaches the target. The coupling potential $\mathcal{F}_{cc'}$ is defined by

$$\mathcal{F}_{cc'}(b,z) = \langle\varphi_c|U_{14} + U_n - V_{\mathrm{C}}|\varphi_{c'}\rangle_{\boldsymbol{r}}e^{i(m-m')\phi_R}, \quad (13)$$

and

$$\mathcal{R}_{ii'}(b,z) = \frac{(K_{i'}R - K_{i'}z)^{i\eta_{i'}}}{(K_iR - K_iz)^{i\eta_i}}. \quad (14)$$

Within the E-CDCC framework, the boundary condition Eq. (4) translates into

$$\lim_{z\to-\infty}\bar{\xi}_{i\ell m}(b,z) = \delta_{i0}\delta_{\ell\ell_0}\delta_{mm_0}. \quad (15)$$

C. Dynamical eikonal approximation

In the DEA, the three-body wave function is factorized following [16,17]

$$\Psi(\boldsymbol{R},\boldsymbol{r}) = \psi(\boldsymbol{b},z,\boldsymbol{r})e^{iK_0z}e^{i\chi_{\mathrm{C}}(b,z)}e^{i\varepsilon_0 z/(\hbar v_0)}, \quad (16)$$

where χ_{C} is the Coulomb phase that accounts for the Coulomb projectile-target scattering

$$\chi_{\mathrm{C}}(b,z) = -\frac{1}{\hbar v_0}\int_{-\infty}^{z}V_{\mathrm{C}}(R)\,dz', \quad (17)$$

where $v_0 = \hbar K_0/\mu$ is the initial velocity of the projectile. Note that the phase $\exp[\varepsilon_0 z/(i\hbar v_0)]$ can be ignored as it has no effect on physical observables [17].

From the factorization in Eq. (16), we obtain the DEA equation [16,17]

$$i\hbar v_0\frac{\partial}{\partial z}\psi(\boldsymbol{b},z,\boldsymbol{r}) = [h + U_{14} + U_n - \varepsilon_0 - V_{\mathrm{C}}]\psi(\boldsymbol{b},z,\boldsymbol{r}). \quad (18)$$

The initial condition of Eq. (4) translates into

$$\lim_{z\to-\infty}\psi(\boldsymbol{b},z,\boldsymbol{r}) = \varphi_{0\ell_0m_0}(\boldsymbol{r}). \quad (19)$$

The DEA equation (18) is solved for all $\boldsymbol{b}$ with respect to z and $\boldsymbol{r}$ expanding the wave function ψ on a three-dimensional mesh. This allows to include naturally all relevant states of ^{15}C, i.e., eigenenergies ε up to high values in the n-^{14}C continuum, and large angular momentum ℓ, and its z-component m. This resolution is performed assuming a constant projectile-target relative velocity $v = v_0$. It should be noted that this does not mean the adiabatic approximation, because in Eq. (18) the internal Hamiltonian h is explicitly included. The DEA thus treats properly the change in the eigenenergy of ^{15}C during the scattering process. However, it does not change the ^{15}C-^{208}Pb velocity accordingly. This gives a violation of the conservation of the total energy of the three-body system. However, even at 20 MeV/nucleon, its effect is expected to be only a few percent as discussed below.

The calculation of physical observables requires the wave function Ψ of Eq. (16) at $z \to \infty$ [16,17]. The corresponding Coulomb phase χ_{C} reads [25]

$$\lim_{z\to\infty}\chi_{\mathrm{C}} = 2\eta_0\ln(K_0b), \quad (20)$$

where η_0 is the Sommerfeld parameter for the entrance channel [see Eq. (9)].

D. Comparison between E-CDCC and DEA

To ease the comparison between the DEA and the E-CDCC, we rewrite the formulas given in Sec. II C in a coupled-channel

representation. We expand ψ as

$$\psi(\boldsymbol{b},z,\boldsymbol{r}) = \sum_{i\ell m} \xi_{i\ell m}(b,z)\varphi_{i\ell m}(\boldsymbol{r})e^{\varepsilon_i z/(i\hbar v_0)}e^{i(m_0-m)\phi_R}. \quad (21)$$

Inserting Eq. (21) into Eq. (18), multiplied by $\varphi_{i'\ell'm'}$ from the left, and integrating over $\boldsymbol{r}$, one gets

$$\frac{\partial}{\partial z}\xi_c(b,z) = \frac{1}{i\hbar v_0}\sum_{c'} \mathcal{F}_{cc'}(b,z)\xi_{c'}(b,z)e^{(\varepsilon_{i'}-\varepsilon_i)z/(i\hbar v_0)}, \quad (22)$$

which is nothing but the DEA equation (18) in its coupled-channel representation.

The boundary condition Eq. (19) thus reads

$$\lim_{z\to-\infty} \xi_{i\ell m}(b,z) = \delta_{i0}\delta_{\ell\ell_0}\delta_{mm_0}. \quad (23)$$

Considering the expansion Eq. (21) in the DEA factorization Eq. (16), the total wave function reads

$$\Psi(\boldsymbol{R},\boldsymbol{r}) = \sum_c \xi_c(b,z)\varphi_c(\boldsymbol{r})e^{(\varepsilon_i-\varepsilon_0)z/(i\hbar v_0)} \times e^{i(m_0-m)\phi_R}e^{iK_0 z}e^{i\chi_C(b,z)}. \quad (24)$$

One may summarize the difference between Eqs. (22) and (10) as follows. First, the DEA uses the constant and channel-independent ^{15}C-^{208}Pb relative velocity v_0, whereas E-CDCC uses the velocity depending on both R and the channel i that ensures the total-energy conservation.

Second, whereas the right-hand side of Eq. (22) involves the phase $\exp[(\varepsilon_{i'}-\varepsilon_i)z/(i\hbar v_0)]$, the E-CDCC Eq. (10) includes the phase $\exp[i(K_{i'}-K_i)z]$. The former can be rewritten as

$$\frac{\varepsilon_{i'}-\varepsilon_i}{i\hbar v_0}z = \frac{\hbar^2\left(K_i^2-K_{i'}^2\right)}{2\mu}\frac{\mu z}{i\hbar^2 K_0} = \frac{K_{i'}+K_i}{2K_0}i(K_{i'}-K_i)z. \quad (25)$$

If we can assume the semi-adiabatic approximation

$$\frac{K_{i'}+K_i}{2K_0} \approx 1, \quad (26)$$

the exponent Eq. (25) becomes the same as in E-CDCC. In the model space taken in the present study, Eq. (26) holds within 1.5% error at 20 MeV/nucleon of incident energy.

Third, E-CDCC equation contains $\mathcal{R}_{ii'}$ taking account of the channel dependence of the ^{15}C-^{208}Pb Coulomb wave function, which DEA neglects. Nevertheless, it should be noted that, as shown in Refs. [14,15], the Coulomb wave functions in the initial and final channels involved in the transition matrix (T matrix) of E-CDCC eventually give a phase $2\eta_j \ln(K_j b)$, with j the energy index in the final channel. Thus, if Eq. (26) holds, the role of the Coulomb wave function in the evaluation of the T matrix in E-CDCC is expected to be the same as in DEA, since DEA explicitly includes the Coulomb eikonal phase, Eq. (20).

When the Coulomb interaction is absent, we have $\mathcal{R}_{ii'}(b,z) = 1$ and no R dependence of the velocity. Therefore, it will be interesting to compare the results of DEA and E-CDCC with and without the Coulomb interaction separately.

TABLE I. Potential parameters for the pair interactions $U_{n\mathrm{C}}$, U_{14}, and U_n [23].

	V_0 (MeV)	R_0 (fm)	a_0 (fm)	W_v (MeV)	W_s (MeV)	R_w (fm)	a_w (fm)	R_C (fm)
$U_{n\mathrm{C}}$	63.02	2.651	0.600	-	-	-	-	-
U_{14}	50.00	9.844	0.682	50.00	-	9.544	0.682	10.84
U_n	44.82	6.932	0.750	2.840	21.85	7.466	0.580	-

III. RESULTS AND DISCUSSION

A. Model setting

We calculate the energy spectrum $d\sigma/d\varepsilon$ and the angular distribution $d\sigma/d\Omega$ of the breakup cross section of ^{15}C on ^{208}Pb at 20 MeV/nucleon, where ε is the relative energy between n and ^{14}C after breakup, and Ω is the scattering angle of the c.m. of the n-^{14}C system. We use the potential parameters shown in Table I for $U_{n\mathrm{C}}$ (the n-^{14}C interaction), U_{14}, and U_n [23]; the depth of $U_{n\mathrm{C}}$ for the d-wave is changed to 69.43 MeV to avoid a nonphysical d resonance. The spin of the neutron is disregarded as mentioned earlier. We adopt Woods-Saxon potentials for the interactions

$$U_x(R_x) = -V_0 f(R_x,R_0,a_0) - iW_v f(R_x,R_w,a_w) + iW_s\frac{d}{dR_x}f(R_x,R_w,a_w), \quad (27)$$

with $f(R_x,\alpha,\beta) = (1+\exp[(R_x-\alpha)/\beta])^{-1}$; $R_x = r$, R_{14}, and R_n for $x = n\mathrm{C}$, 14, and n, respectively. The Coulomb interaction between ^{14}C and ^{208}Pb is described by assuming a uniformly charged sphere of radius R_C.

Unless stated otherwise, the model spaces chosen for our calculations give a confidence level better than 3% on the cross sections presented in Secs. III B and III C. In E-CDCC, we take the maximum value of r to be 800 fm with the increment of 0.2 fm. When the Coulomb interaction is turned off, we take the n-^{14}C partial waves up to $\ell_{\max} = 10$. For each ℓ the continuum state is truncated at $k_{\max} = 1.4$ fm^{-1} and discretized into 35 states with the equal spacing of $\Delta k = 0.04$ fm^{-1}; k is the relative wave number between n and ^{14}C. The resulting number of coupled channels, N_{ch}, is 2311. The maximum values of z and b, $z_{\max}$ and $b_{\max}$, respectively, are both set to 50 fm. When the Coulomb interaction is included, we use $\ell_{\max} = 6$, $k_{\max} = 0.84$ fm^{-1}, $\Delta k = 0.04$ fm^{-1}, $z_{\max} = 1000$ fm, and $b_{\max} = 150$ fm. We have $N_{\mathrm{ch}} = 589$ in this case.

In the DEA calculations, we use the same numerical parameters as in Ref. [23]. In the purely nuclear case, the wave function ψ is expanded over an angular mesh containing up to $N_\theta \times N_\varphi = 14 \times 27$ points, a quasi-uniform radial mesh that extends up to 200 fm with 200 points, $b_{\max} = 50$ fm, and $z_{\max} = 200$ fm (see Ref. [26] for details). In the charged case, the angular mesh contains up to $N_\theta \times N_\varphi = 12 \times 23$ points, the radial mesh extends up to 800 fm with 800 points, $b_{\max} = 300$ fm, and $z_{\max} = 800$ fm.

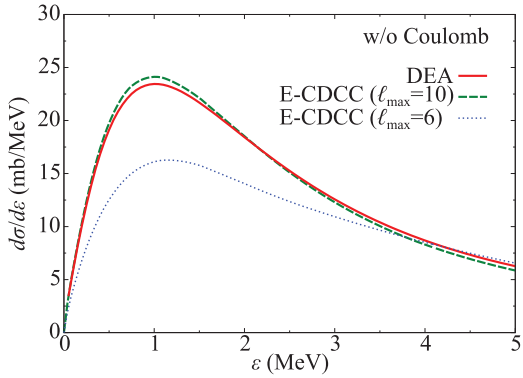

FIG. 2. (Color online) Energy spectrum of the ^{15}C breakup cross section on ^{208}Pb at 20 MeV/nucleon with the Coulomb interaction turned off. The solid and dashed lines show the results obtained by DEA and E-CDCC, respectively. The result of E-CDCC with $\ell_{max} = 6$ is denoted by the dotted line.

B. Comparison without Coulomb interaction

The goal of the present work being to study the difference in the treatment of the Coulomb breakup between the E-CDCC and DEA, we first check that both models agree when the Coulomb interaction is switched off. We show in Fig. 2 the results of $d\sigma/d\varepsilon$ calculated by DEA (solid line) and E-CDCC (dashed line); $d\sigma/d\varepsilon$ is obtained by integrating the double-differential breakup cross section $d^2\sigma/(d\varepsilon d\Omega)$ over Ω in the whole variable region. The two results agree very well with each other; the difference around the peak is below 3%.

In Fig. 3 the comparison in $d\sigma/d\Omega$, i.e., $d^2\sigma/(d\varepsilon d\Omega)$ integrated over ε up to 10 MeV, is shown. The agreement between the two models is excellent confirming that, when the Coulomb interaction is turned off, the DEA and E-CDCC solve the same equation and give the same result, as expected from the discussion at the end of Sec. II D. In particular this comparison shows that Eq. (26) turns out to be satisfied with very high accuracy. It should be noted that the good agreement between the DEA and E-CDCC is obtained only when a very large model space is taken. In fact, if we put $\ell_{max} = 6$ in E-CDCC, we have 30% smaller $d\sigma/d\varepsilon$ (dotted line) than the converged value and, more seriously, even the shape cannot be reproduced. This result shows the importance of the higher partial waves of n-^{14}C for the nuclear breakup at 20 MeV/nucleon.

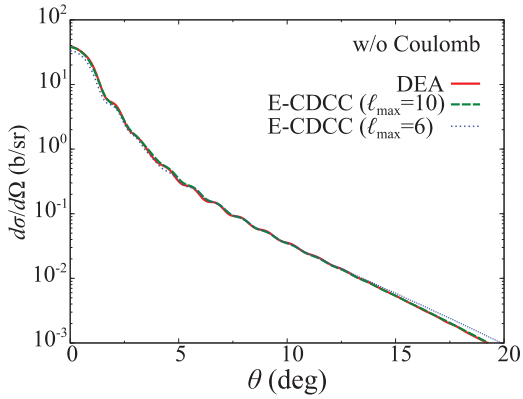

FIG. 3. (Color online) Same as Fig. 2 but for the angular distribution.

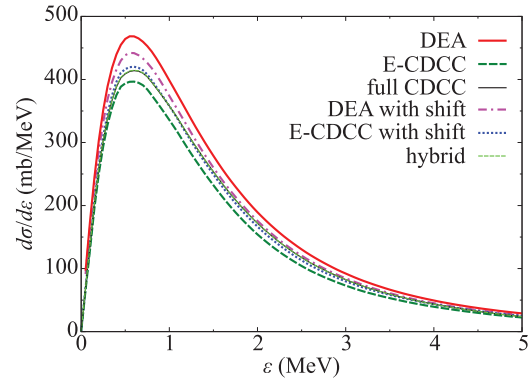

FIG. 4. (Color online) Energy spectrum of the ^{15}C breakup cross section on ^{208}Pb at 20 MeV/nucleon including the Coulomb interaction. The solid, dashed, and thin solid lines show the results obtained by DEA, E-CDCC, and full (QM) CDCC, respectively. The results obtained with the correction (28) are displayed with a dash-dotted line for DEA and a dotted line for E-CDCC. The calculation using the QM correction of E-CDCC, i.e., the hybrid calculation, is shown by the light-green thin dashed line (superimposed onto the thin solid line).

C. Comparison to Coulomb interaction

When the Coulomb interaction is switched on, DEA and E-CDCC no longer agree with each other. As seen in Fig. 4, the DEA energy spectrum (solid line) is much larger than the E-CDCC one (dashed line). Moreover none of them agrees with the full CDCC calculation (thin solid line): DEA is too high while E-CDCC is too low. The discrepancy of both models with the fully quantal calculation manifests itself even more clearly in the angular distribution. In Fig. 5 we see that not only do the DEA and E-CDCC cross sections differ in magnitude, but—as already seen in Ref. [23]—their oscillatory pattern is shifted to forward angle compared to the CDCC calculation. To understand where the problem comes from we analyze in Fig. 6 the contribution to the total breakup cross section

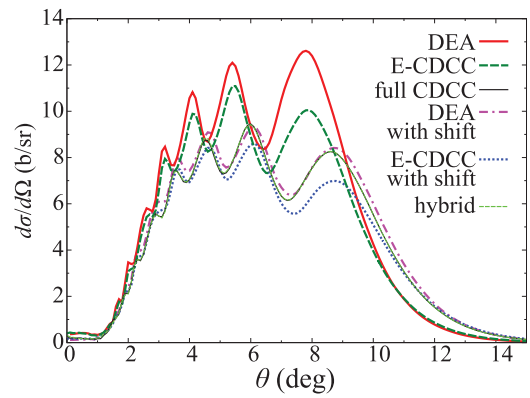

FIG. 5. (Color online) Same as Fig. 4 but for the angular distribution.

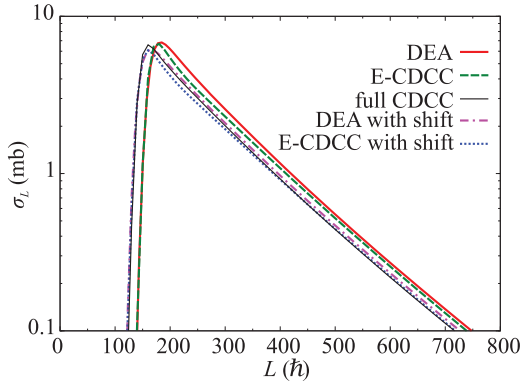

FIG. 6. (Color online) Contribution to the total breakup cross section per projectile-target angular momentum L. Neglecting the Coulomb deflection, DEA and E-CDCC are shifted to large L compared to the full CDCC. The correction Eq. (28) significantly reduces this shift for both models.

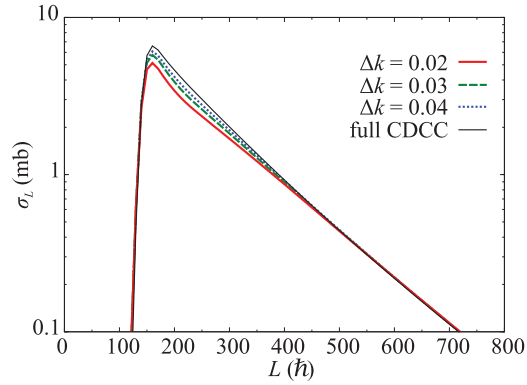

FIG. 7. (Color online) Convergence problem observed in (shifted) E-CDCC calculations: cross sections computed with different bin widths do not converge towards the CDCC calculation.

of each projectile-target relative angular momentum L. As expected from Figs. 4 and 5, the DEA calculation is larger than the E-CDCC one, and this is observed over the whole L range. However, the most striking feature is to see that both models seem to be shifted to larger L compared to the full CDCC calculation. To correct this, we replace in our calculations the transverse component of the projectile-target relative coordinate b by the empirical value [25,27,28]

$$b' = \frac{\eta_0}{K_0} + \sqrt{\frac{\eta_0^2}{K_0^2} + b^2}. \tag{28}$$

The corresponding results are displayed in Figs. 4, 5, and 6 as dash-dotted lines for DEA and dotted lines for E-CDCC.

The correction Eq. (28) is very effective. It significantly reduces the shift observed in the L contributions to the breakup cross section (see Fig. 6). Accordingly, it brings both DEA and E-CDCC energy spectra closer to the full CDCC one (see Fig. 4). Note that for this observable the correction seems better for E-CDCC than for DEA: even with the shift, the latter still exhibits a nonnegligible enhancement with respect to CDCC at low energy E. More spectacular is the correction of the shift in the angular distribution observed in Ref. [23] and in Fig. 5. In particular, the shifted DEA cross section is now very close to the CDCC one, but at forward angles, where DEA overestimates CDCC. Once shifted, E-CDCC still underestimates slightly the full CDCC calculation. However, its oscillatory pattern is now in phase with that of the CDCC cross section, which is a big achievement in itself. This shows that the lack of Coulomb deflection observed in Ref. [23] for eikonal-based calculations can be efficiently corrected by the simple shift Eq. (28) suggested long ago [25,28].

Albeit efficient, the correction Eq. (28) is not perfect. This is illustrated by the enhanced (shifted) DEA cross section observed in the low-energy peak in Fig. 4 and at forward angles in Fig. 5. Both problems can be related to the same root because the forward-angle part of the angular distribution is dominated by low-energy contributions. As shown in Ref. [17], that part of the cross section is itself dominated by large b's, at which the correction Eq. (28) is not fully sufficient. As shown in Fig. 6, the shifted DEA remains slightly larger than the full CDCC. Future works may suggest a better way to handle this shift than the empirical correction Eq. (28). Nevertheless, these results show that this correction provides a simple, elegant, and cost-effective way to account for Coulomb deflection in eikonal-based models.

The underestimation of the full CDCC angular distribution by E-CDCC comes most likely from a convergence problem within that reaction model. This is illustrated in Fig. 7, showing the L contribution to the total breakup cross section. The thin solid line corresponds to the (converged) CDCC calculation, whereas the other lines correspond to (shifted) E-CDCC calculations with bin widths of $\Delta k = 0.02$ (solid line), 0.03 (dashed line), and 0.04 fm^{-1} (dotted line). As can be seen, below $L \approx 500\hbar$ no convergence can be obtained, although CDCC has fully converged. We cannot expect this model to provide accurate breakup cross sections. The results displayed in Figs. 4 and 5 are therefore unexpectedly good. Note that the present ill-behavior of E-CDCC occurs only when the Coulomb interaction involved is strong and the incident energy is low; no such behavior was observed in previous studies [6,14,15,19,20]. Interestingly, DEA does not exhibit such a convergence issue. This is reminiscent of the work of Dasso *et al.* [29], where it was observed that reaction calculations converge faster by expanding the wave function upon a mesh rather than by discretization of the continuum.

The aforementioned results indicate that the shift Eq. (28) corrects efficiently for the Coulomb deflection, which is expected to play a significant role at large L. At small L, we believe the nuclear projectile-target interaction will induce significant couplings between various partial waves, which cannot be accounted for by that simple correction. To include these couplings, a hybrid solution between E-CDCC and the full CDCC has been suggested [14,15]. At low L a usual CDCC calculation is performed, which fully accounts for the strong coupling expected from the nuclear interaction between the projectile and the target. At larger L, these couplings are expected to become negligible, which implies that a (shifted) E-CDCC calculation should be reliable. As explained in Refs. [14,15], the transition angular momentum L_C above

which E-CDCC is used is an additional parameter of the model space that has to be determined in the convergence analysis. Depending on the beam energy and the system studied, usual values of L_C are in the range 400–1000$\hbar$. In the present case, due to the convergence issue observed in E-CDCC, the value $L_C = 500\hbar$ is chosen.

The quality of this hybrid solution is illustrated by the light-green thin dashed lines in Figs. 4 and 5, which are barely visible as they are superimposed to the full CDCC results. The coupling of the hybrid solution to the Coulomb shift Eq. (28) enables us to reproduce exactly the CDCC calculations at a much lower computational cost since the computational time for each b with E-CDCC is about 1/60 of that for each L with full CDCC. In addition, it solves the convergence problem of E-CDCC.

IV. SUMMARY

With the ultimate goal of understanding the ability of the hybrid version of the continuum-discretized coupled-channels method with the eikonal approximation (E-CDCC) to account for the discrepancy between the dynamical eikonal approximation (DEA) and the continuum discretized coupled-channel model (CDCC) observed in Ref. [23], we have clarified the relation between the DEA and E-CDCC. By using a coupled-channel representation of DEA equations, DEA is shown to be formally equivalent to E-CDCC, if the semi-adiabatic approximation of Eq. (26) is satisfied and the Coulomb interaction is absent.

We consider the same test case as in Ref. [23], i.e., the breakup of ^{15}C on ^{208}Pb at 20 MeV/nucleon. For this reaction Eq. (26) holds within 1.5% error. When the Coulomb interaction is artificially turned off, DEA and E-CDCC are found to give the same result within 3% difference for both the energy spectrum and the angular distribution. This supports the equivalence of the two models for describing the breakup process due purely to nuclear interactions.

Next we make a comparison including the Coulomb interaction. In this case, DEA and E-CDCC no longer agree with each other and they both disagree with the full CDCC calculation. In particular, both angular distributions are focused at too forward an angle, as reported in Ref. [23]. This lack of Coulomb deflection of the eikonal approximation can be solved using the empirical shift Eq. (28). Using this shift the agreement with CDCC improves significantly.

In addition, E-CDCC turns out to have a convergence problem, which indicates the limit of application of the eikonal approximation using a discretized continuum to reactions at such low energies involving a strong Coulomb interaction. Fortunately, by including a QM correction to E-CDCC for lower projectile-target partial waves, this convergence problem is completely resolved. Moreover, the result of this hybrid calculation perfectly agrees with the result of the full (QM) CDCC.

The present study confirms the difficulty to properly describe the Coulomb interaction within the eikonal approximation at low energy. However, it is found that even at 20 MeV/nucleon, the empirical shift Eq. (28) helps correctly reproducing the Coulomb deflection that was shown to be missing in the DEA [23]. Including QM corrections within the E-CDCC leads to a hybrid model that exhibits the same accuracy as the full CDCC, with a minimal computational cost. This hybrid calculation will be useful for describing nuclear and Coulomb breakup processes in a wide range of incident energies. It could be included in other CDCC programs to increase their computational efficiency without reducing their accuracy. This could be an asset to improve the description of projectiles while keeping reasonable calculation times.

ACKNOWLEDGMENTS

The authors thank D. Baye and M. Yahiro for valuable comments on this study. This research was supported in part by the Fonds de la Recherche Fondamentale Collective (Grant No. 2.4604.07F), Grant-in-Aid of the Japan Society for the Promotion of Science (JSPS), and RCNP Young Foreign Scientist Promotion Program. This paper presents research results of the Belgian Research Initiative on eXotic nuclei (BRIX), Program No. P7/12, on interuniversity attraction poles of the Belgian Federal Science Policy Office.

[1] I. Tanihata, J. Phys. G **22**, 157 (1996).
[2] B. Jonson, Phys. Rep. **389**, 1 (2004).
[3] D. Baye and P. Capel, *Breakup Reaction Models for Two- and Three-Cluster Projectiles in Cluster in Nuclei, Vol. 2*, Lecture Notes in Physics 848, edited by C. Beck (Springer, Berlin, 2012), p. 121.
[4] M. Kamimura, M. Yahiro, Y. Iseri, Y. Sakuragi, H. Kameyama, and M. Kawai, Prog. Theor. Phys. Suppl. No. **89**, 1 (1986).
[5] N. Austern, Y. Iseri, M. Kamimura, M. Kawai, G. Rawitscher, and M. Yahiro, Phys. Rep. **154**, 125 (1987).
[6] M. Yahiro, K. Ogata, T. Matsumoto, and K. Minomo, Prog. Theor. Exp. Phys. **2012**, 01A206 (2012), and references therein.
[7] N. Austern, M. Yahiro, and M. Kawai, Phys. Rev. Lett. **63**, 2649 (1989).
[8] N. Austern, M. Kawai, and M. Yahiro, Phys. Rev. C **53**, 314 (1996).
[9] A. M. Moro, J. M. Arias, J. Gómez-Camacho, I. Martel, F. Pérez-Bernal, R. Crespo, and F. Nunes, Phys. Rev. C **65**, 011602(R) (2001).
[10] T. Matsumoto, T. Kamizato, K. Ogata, Y. Iseri, E. Hiyama, M. Kamimura, and M. Yahiro, Phys. Rev. C **68**, 064607 (2003).
[11] T. Egami, K. Ogata, T. Matsumoto, Y. Iseri, M. Kamimura, and M. Yahiro, Phys. Rev. C **70**, 047604 (2004).
[12] M. Rodríguez-Gallardo, J. M. Arias, J. Gómez-Camacho, A. M. Moro, I. J. Thompson, and J. A. Tostevin, Phys. Rev. C **80**, 051601 (2009).
[13] R. J. Glauber, in *High Energy Collision Theory*, Lectures in Theoretical Physics, Vol. 1, edited by W. E. Brittin and L. G. Dunham (Interscience, New York, 1959), p. 315.

[14] K. Ogata, M. Yahiro, Y. Iseri, T. Matsumoto, and M. Kamimura, Phys. Rev. C **68**, 064609 (2003).
[15] K. Ogata, S. Hashimoto, Y. Iseri, M. Kamimura, and M. Yahiro, Phys. Rev. C **73**, 024605 (2006).
[16] D. Baye, P. Capel, and G. Goldstein, Phys. Rev. Lett. **95**, 082502 (2005).
[17] G. Goldstein, D. Baye, and P. Capel, Phys. Rev. C **73**, 024602 (2006).
[18] Y. Suzuki, R. G. Lovas, K. Yabana, and K. Varga, *Structure and Reactions of Light Exotic Nuclei* (Taylor and Francis, London, 2003).
[19] K. Ogata and C. A. Bertulani, Prog. Theor. Phys. **121**, 1399 (2009).
[20] K. Ogata and C. A. Bertulani, Prog. Theor. Phys. **123**, 701 (2010).
[21] M. Yahiro, K. Ogata, and K. Minomo, Prog. Theor. Phys. **126**, 167 (2011).
[22] S. Hashimoto, M. Yahiro, K. Ogata, K. Minomo, and S. Chiba, Phys. Rev. C **83**, 054617 (2011).
[23] P. Capel, H. Esbensen, and F. M. Nunes, Phys. Rev. C **85**, 044604 (2012).
[24] M. Yahiro, Y. Iseri, H. Kameyama, M. Kamimurai, and M. Kawai, Prog. Theor. Phys. Suppl. No. **89**, 32 (1986).
[25] C. A. Bertulani and P. Danielewicz, *Introduction to Nuclear Reactions* (Institute of Physics, Bristol, England, 2004).
[26] P. Capel, D. Baye, and V. S. Melezhik, Phys. Rev. C **68**, 014612 (2003).
[27] C. A. Bertulani, C. M. Campbell, and T. Glasmacher, Comp. Phys. Comm. **152**, 317 (2003).
[28] R. A. Broglia and A. Winther, *Heavy Ion Reactions, Lectures Notes, Vol. 1: Elastic and Inelastic Reactions* (Benjamin/Cummings, Reading, England, 1981).
[29] C. H. Dasso and A. Vitturi, Phys. Rev. C **79**, 064620 (2009).